Effects of Orography on the Generation and Propagation of Mesoscale Convective Systems in a Two-Dimensional Conditionally Unstable Flow

CHANG-MIN CHU AND YUH-LANG LIN

Department of Marine, Earth and Atmospheric Sciences, North Carolina State University, Raleigh, North Carolina

(Manuscript received 20 May 1998, in final form 1 April 2000)

ABSTRACT

Effects of orography, cold-air outflow, and gravity waves on the generation and propagation of convective systems in a conditionally unstable airstream over a mesoscale mountain are studied using a two-dimensional cloud model. Based on the propagation of convective systems, three regimes are identified: (I) an upstream propagating convective system, (II) a quasi-stationary convective system, and (III) quasi-stationary and downstream propagating systems. In regime I [low moist Froude number (F_w)], the convective cells are generated by upstream deceleration associated with orographic forcing, by gravity waves associated with convective cells over the upslope area at earlier stages, and by the upstream propagating density current at later stages when the density current is fully developed. In this flow regime, quasi-continuous and heavy rainfall is produced over the upslope and plain areas as individual convective cells develop farther upstream at the head of the density current and then propagate downstream once they form. In regime II (moderate F_w), the convective system becomes quasi-stationary over the upslope and in the vicinity of the mountain peak. The individual convective cells are mainly produced by orographic forcing and gravity waves associated with the mountain-induced convective system. A balance between the orographic forcing and the cold-air outflow forcing has been reached in this flow regime. In addition, the convective cells are able to merge into a large single cell due to the phasing of orographic forcing and gravity wave forcing. In regime III (large F_w), two modes of convective systems are identified: the quasi-stationary and downstream propagating modes. For the quasi-stationary convective system, the formation mechanisms are the same as those in regime II. For the downstream propagating convective system, the convective cells are mainly generated by convergence associated with an internal hydraulic jump over the lee slope.

Without evaporative cooling, the mountain-induced convective system cannot trigger new cells far upstream of the mountain. The dominant convective system is advected downstream slowly by the basic flow. With the presence of upstream deceleration, the convective system tends to occur far upstream on the plain area rather than over the upslope of the mountain.

1. Introduction

The distribution of precipitation locally controlled by orography has been observed in many parts of the world. Formation mechanisms of orographic rain have been proposed by Smith (1979), Houze (1993), and Lin (1993) and may be classified into three main categories: 1) upslope orographic rain in a stable atmosphere, 2) orographic rain in a conditionally unstable atmosphere, and 3) orographic rain induced by the seeder cloud-feeder cloud mechanism. A schematic diagram of formation mechanisms of orographic rain is shown in Fig. 1. Orographic rain in category 2 is often induced by a low-level jet and characterized by closely packed convection. The orographic rain triggered by convergence produced by low-level sensible heating occurred over mountain peak also belongs to this category. The presence of katabatic flow produced by low-level sensible cooling over the mountain at night may also enhance the rainfall. According to the intensive observations in the Taiwan Area Mesoscale Experiment (TAMEX), heaviest rainfalls are favored to occur on the windward slope. However, in some of the observed events, the heavy rainfall occurs on the plain area rather than on the mountain slopes (e.g., Jou 1997). The formation mechanisms of such phenomena are not clear, although some studies have suggested that upstream deceleration is able to trigger heavy rain on the plain area upstream of the mountain (Grossman and Durran 1984; Smolarkiewicz et al. 1988; Hong and Huang 1996).

Smith and Lin (1982) presented a theoretical study of the linear response of a stratified hydrostatic airstream to combined thermal and orographic forcing. Using a prescribed heating distribution to represent the diabatic

Corresponding author address: Dr. Yuh-Lang Lin, Department of Marine, Earth and Atmospheric Sciences, North Carolina State University, Raleigh, NC 27695-8208.
E-mail: yl_lin@ncsu.edu

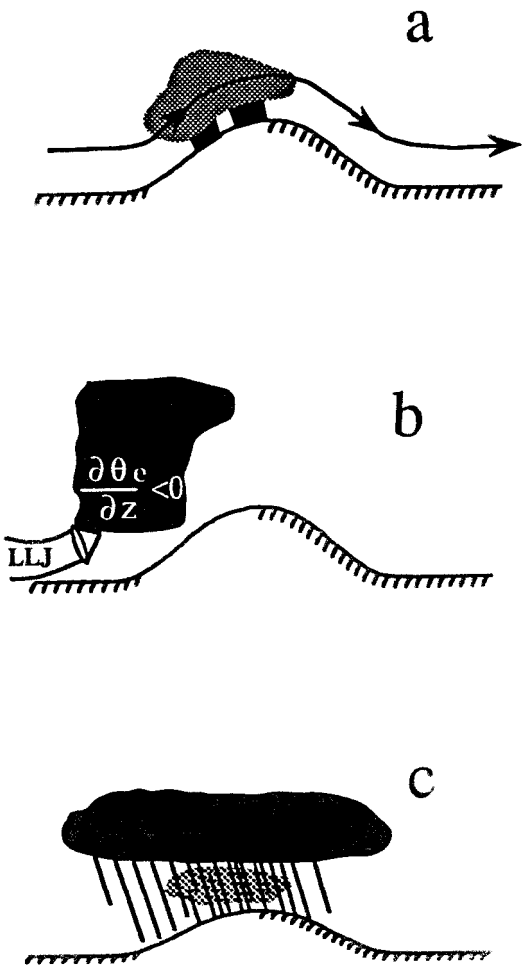

FIG. 1. A sketch of the formation mechanisms of orographic rain: (a) upslope orographic rain in a stable atmosphere, (b) orographic rain in a conditionally unstable atmosphere, and (c) orographic rain induced by seeder cloud-feeder cloud mechanism. Orographic rain in category 2 is often associated with closely packed convection and may be induced by either a low-level jet carrying warm and moist air or convergence associated with low-level sensible heating or cooling. (Modified from Smith 1979 and Lin 1993.)

effects of a precipitating orographic cloud, they found that thermally generated waves could equal or even exceed orographically generated waves for typical wind speeds and rainfall rates. However, the dynamics for low–Froude number, moist flow over a mountain may be very different and deserve further study. Studies of thunderstorm outflow suggest that the density current produced by the evaporation of falling precipitation in the subcloud layer may serve as a formation mechanism for convective storms (e.g., Thorpe et al. 1982; Droegemeier and Wilhelmson 1987; Mueller and Carbone 1987). It is therefore important to account for the combined effects of cold-air outflow and orographic forcing on the generation of convective systems.

Raymond and Rotunno (1989) studied the formation of a density current in a dry, uniform, stably stratified flow in response to prescribed cooling. Four flow regimes were categorized by using the nondimensional parameters, $F = |U|/(Qdl)^{1/3}$ and $G = \pi|U|/Nd$, where Q is the cooling rate and d and l are the depth and width of the cooling region. The parameter $(Qdl)^{1/3}$ roughly represents the speed of the propagating density current, and Nd/π is the horizontal trace speed (in still air) of hydrostatic gravity waves with a vertical wavelength $2d$. Lin and Chun (1991) extended Raymond and Rotunno's work to a stably stratified shear flow with a critical level. They found that the response of the atmosphere to steady cooling in a shear flow may be categorized as either a stationary cold pool or a density current, depending upon the strength of the effective cooling. If we consider a moist flow over a mountain, then a moist Froude number may be defined as $F_w = U/N_w h$, where U is the basic wind speed, N_w is the moist Brunt–Väisälä frequency, and h is the mountain height. In this study, we are interested in identifying moist flow regimes based on F_w by a series of numerical simulations.

The convergence associated with the deceleration of a fluid as it impinges on a mountain tends to induce ascent, which in turn is capable of producing deep convection and heavy rainfall on the plain area upstream of the mountain. Lin and Wang (1996) proposed four regimes for a two-dimensional, dry, unstructured, nonrotating, continuously stratified, hydrostatic, uniform, Boussinesq flow over an isolated mountain: (LW-I) flow with neither wave breaking aloft nor upstream blocking ($F \geq 1.12$); (LW-II) flow with wave breaking aloft in the absence of upstream blocking ($0.9 < F \leq 1.12$); (LW-III) flow with both wave breaking and upstream blocking, but where wave breaking occurs first ($0.6 < F \leq 0.9$); and (LW-IV) flow with both wave breaking and upstream blocking, but where wave blocking occurs first ($0.3 \leq F \leq 0.6$). Note that in low–Froude number flow, nonlinear effects are stronger because the strength of nonlinearity is inversely proportional to the Froude number. Since some mesoscale mountains, such as the North American Rocky Mountains, the European Alps, Taiwan's Central Mountain Range (CMR), and New Zealand's Alps, are higher than 2 km, the effect of nonlinearity cannot be ignored. For example, the Froude number for airflow with $U = 10$ m s^{-1} and $N = 0.01$ s^{-1} over Taiwan's CMR ($h = 4$ km) is 0.25, which falls into the regime with upstream blocking and may produce a mesoscale convective system in a conditionally unstable airflow. Thus, the effect of upstream blocking on a moist airstream needs to be investigated.

It was observed that mountain-induced precipitation systems developed continuously on the western slope of the mountains in northwestern Taiwan during the afternoon of 7 June 1987 during TAMEX (Chen et al. 1991). The entire convective system propagated downstream at later times. On the other hand, in a pilot program of the TAMEX Forecast Experiment in 1991, Jou (1994) found the convective systems produced over the mountain ridge in northern Taiwan propagated against

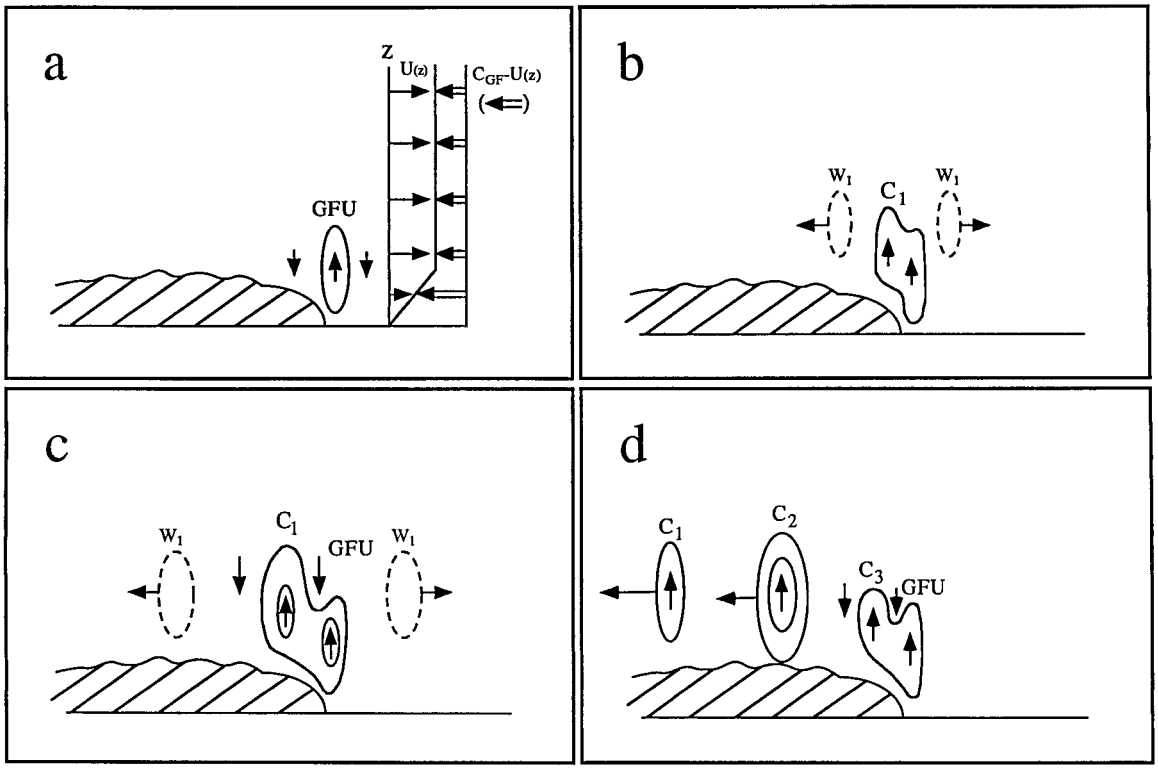

FIG. 2. A schematic model for cell regeneration and propagation within a two-dimensional multicell thunderstorm. Four stages are found: (a) formation and maintenance of the gust front updraft (GFU); (b) rearward advection of the growing GFU; (c) cutting off of the growing cell (c_1) from the GFU by the upstream compensating downdraft; (d) cell regeneration and coexistence of the growing (c_2 and c_3) and propagating (c_1) modes. (After Lin et al. 1998.)

the incoming flow toward the Taipei valley. The flow parameters that indicate whether convective systems will exhibit upstream or downstream propagation are still not clear. In addition, the cell regeneration mechanism for an environment conducive to multicell storms in the vicinity of a mountain (e.g., Chen et al. 1991) is also not well understood. Recently, Jou (1997) composed radar images for cases with mesoscale convective systems propagating upstream, remaining stationary, and propagating downstream with respect to the mountain peak. The mechanisms and control parameters responsible for these behaviors remain to be identified.

Mechanisms of cell regeneration, development, and propagation within a two-dimensional multicell storm have been proposed recently by Lin et al. (1998). The cell regeneration is explained by the following mechanism: (i) an updraft (usually called gust front updraft or GFU) is formed by low-level convergence ahead of the gust front near the surface at the edge of the gust front; (ii) the upper portion of the GFU tends to grow upward as well as rearward by the midlevel inflow advection since the gust front propagates faster than the basic wind; (iii) the rear portion of the GFU develops into a growing cell, which tends to produce strong compensating downdrafts on both sides; and (iv) the growing cell is cut off by its upstream compensating downdraft from the GFU. This growing cell then develops into a stronger convective cell while it moves rearward. Figure 2 shows a schematic model for this mechanism. In addition, cell development and propagation within a two-dimensional multicell storm may be described in terms of two distinctive modes: (i) a growing mode and (ii) a propagating mode [similar to Yang and Houze (1995)]. The detailed dynamics of cell development and propagation is explained in Lin et al. (1998) by critical level dynamics. When a growing cell reaches its maximum intensity, it splits and then propagates downstream without amplification. The growth for the growing mode is dictated by the steering level propagation in a conditionally unstable environment, while the lack of growth for the propagation mode is caused by the lack of a critical level in a more stable environment. In this study, we will apply these mechanisms to explain the cell regeneration, development, and propagation within a multicell storm in the vicinity of a mountain.

The objective of this study is to investigate the possible forcing mechanisms for convection and its propagation over mesoscale mountains using a nonlinear cloud model. The current study is not designed to understand multicell thunderstorm evolution over terrain. The numerical model will be briefly described in section 2. In section 3, we will investigate the effects of cold-

air outflow on the generation and propagation of mesoscale convective cells. Based on the propagation of convective systems, different flow regimes are then identified and discussed in section 4. Concluding remarks are given in the final section.

2. Model description and experiment design

a. Model description

The Advanced Regional Prediction System (ARPS) model, which was developed at the Center for Analysis and Prediction of Storms at the University of Oklahoma (Xue et al. 1995), is adopted for this study. ARPS is a fully compressible nonhydrostatic cloud model based on the Arakawa C grid. ARPS adopts a terrain-following vertical coordinate that may be stretched to increase the low-level vertical resolution. The model has open lateral boundaries to allow disturbances to propagate out of the computational domain and can be initialized by either a single vertical sounding or an observed dataset. Both 1.5-order turbulent kinetic energy and subgrid-scale turbulence schemes are used. The model utilizes 2nd-order centered differencing in the vertical and 4th-order centered differencing in the horizontal. Leapfrog time differencing is employed and the split-explicit scheme is used to treat the gravity waves and acoustic waves. The microphysics of the ARPS model includes the Kessler warm rain parameterization and the Lin–Farley–Orville ice microphysics parameterization scheme, which includes interactions between water vapor, cloud water, cloud ice, rain, snow, and hail. In all the simulations, we assume an inviscid fluid and free-slip lower boundary condition at the surface. The model variables are split into a time-independent, horizontally homogeneous base state-and a time-dependent deviation from the base state. The prognostic perturbation variables include u, v, w, θ, p, and mixing ratios of water vapor, cloud water, rainwater, cloud ice, snow, and hail. The details of the model can be found in Xue et al. (1995).

b. Initial conditions

The initial conditions are obtained by analytic expressions, which were used by Weisman and Klemp (1982). The environmental potential temperature $\overline{\theta}$ and the relative humidity R were given by

$$\overline{\theta}(z) = \begin{cases} \theta_0 + (\theta_{tr} - \theta_0)(z/z_{tr})^{5/4}, & z \le z_{tr} \\ \theta_{tr} \exp[g(z - z_{tr})/c_p T_{tr}], & z > z_{tr} \end{cases} \quad (1)$$

$$R(z) = \begin{cases} 1 - 0.75(z/z_{tr})^{5/4}, & z \le z_{tr} \\ 0.25, & z > z_{tr}, \end{cases} \quad (2)$$

where $z_{tr} = 12$ km, $\theta_{tr} = 343$ K, and $T_{tr} = 213$ K represent the height, potential temperature, and actual temperature, respectively, at the tropopause, and $\theta_0 = 300$ K is the surface potential temperature. The mixing ratio is kept constant at a maximum value q_{v0} near the surface to approximate a well-mixed boundary layer ($\sim$1200 m). The wind profile is uniform in the vertical but is varied in order to obtain different Froude numbers. The vertical profiles of temperature and dewpoints used in this study are shown in Fig. 3. We change the value of θ_0 to obtain different values of convective available potential energy (CAPE).

c. Experimental design

In this study, we are interested in a conditionally unstable airstream over a mesoscale mountain in a uniform wind environment, which may be applicable to a weakly sheared environment in the real atmosphere. In section 4, we choose a two-dimensional, bell-shaped mountain ridge, which may represent an idealized orography of Taiwan. The mountain profile is given by

$$h(x) = \frac{h}{(x/a)^2 + 1}, \quad (3)$$

where h and a are the mountain height and half-width, respectively. The mountain is introduced impulsively in the basic flow at $t = 0$ s. The parameters h, a, Δx, and Δy used in the numerical experiments are 2, 30, 2.5, and 2.5 km, respectively. The grid interval in the vertical direction is stretched from 200 m at the lowest level to 1100 m near the domain top. The domain grid points are 403, 4, and 43 in x, y, and z directions, where the height of physical domain is 16 km. The sponge layer extends from 16 to 25 km.

Since our simulations include moist processes, the averaged Brunt–Väisäla frequency (N_w) and background wind speed (U) far upstream are used to calculate the moist Froude number $F_w = (U/N_w h)$. The moist Brunt–Väisälä frequency is roughly estimated from the surface to 850 mb (Fig. 3), which is presented in the appendix.

The numerical experiments are designed as follows. First, we consider a series of numerical experiments of multicell storms over a flat terrain to investigate the effects of evaporative cooling associated with precipitation on the formation and propagation of the gust front, individual convective cells, and the overall convective system. Second, following the methodology adopted by Lin and Wang (1996), we can determine the critical Froude number (F_c) by using dry simulations. Third, in combined orographic and cold-air outflow forcing, we attempt to classify different flow regimes based on F_w. Fourth, we investigate the effects of evaporative cooling associated with precipitation and upstream deceleration on the generation and propagation of mesoscale convective systems by deactivating the evaporation process.

3. Convective systems induced by cold-air outflow

In order to isolate thunderstorm outflow effects from orographic effects, an axisymmetric thermal perturbation is used in a uniform flow initiated by a single ide-

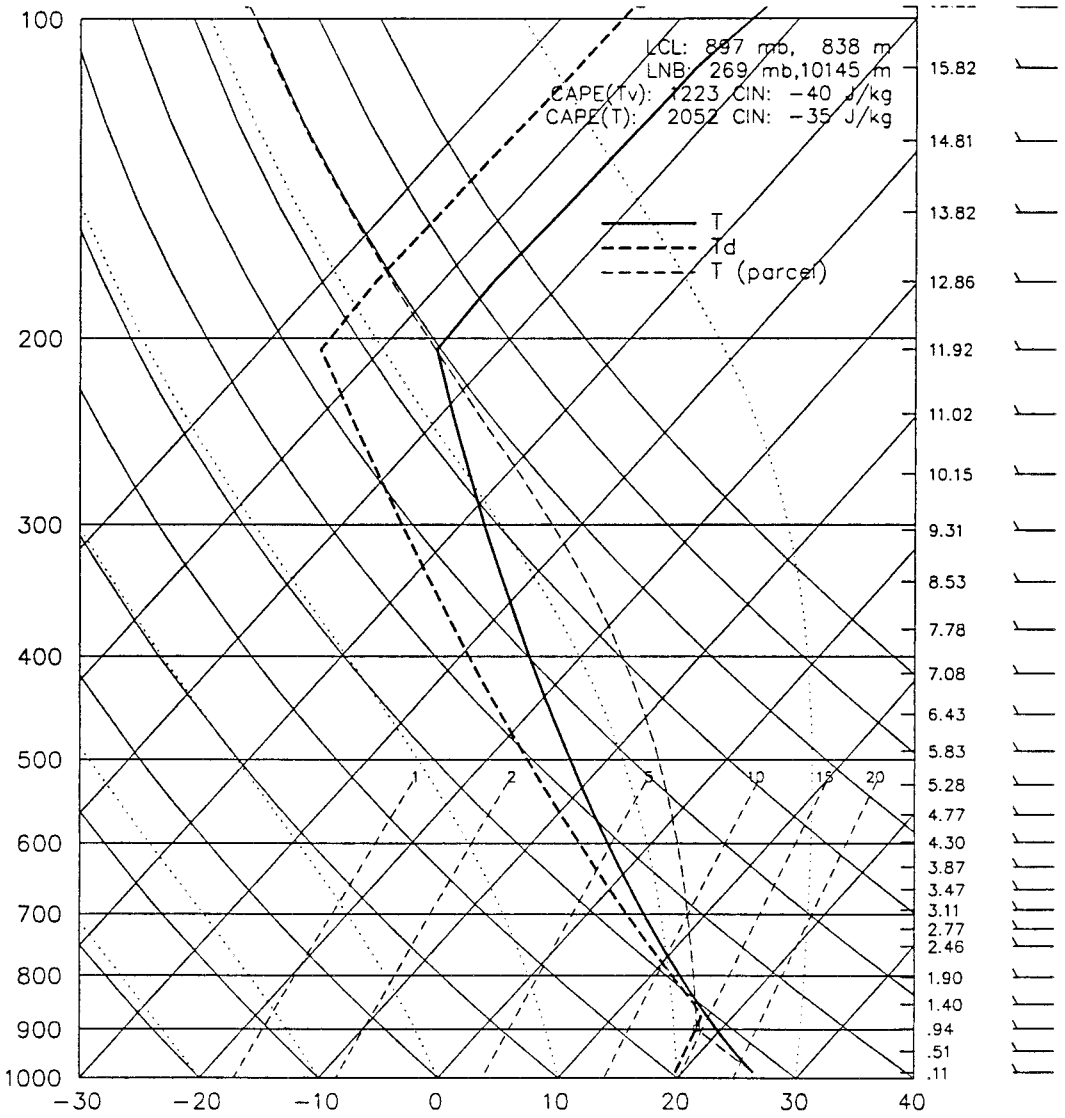

FIG. 3. The idealized sounding used in this study. (After Weisman and Klemp 1982.)

alized sounding. The warm bubble is ellipsoid shaped and defined by

$$\Delta\theta = \theta_0 \cos^2(\pi\beta/2), \qquad \beta \le 1, \tag{4}$$

where θ_0 (=2 K) is the maximum potential temperature at the center of the warm bubble, and β is a nondimensional radius given by

$$\beta = \sqrt{\left(\frac{x - x_c}{x_r}\right)^2 + \left(\frac{z - z_c}{z_r}\right)^2}, \tag{5}$$

where x_c and z_c locate the center of the bubble. In this study, the radii of the bubble are given by $x_r = 10$ km and $z_r = 1.4$ km, respectively. This is similar to Weisman and Klemp (1982), in which they suggested that a temperature perturbation of 2 K represents the minimum value necessary to produce consistent development of an initial convective cell within the experimental range of environmental conditions. A uniform wind profile is used but the wind speed varies from 1 to 15 m s^{-1}. Table 1 summarizes the characteristics of the airflow used in the experiments without orographic forcing.

Figure 4 shows the time evolution of the surface wind speed and rainwater content (q_r) greater than 0.5 g kg^{-1} at $z = 1$ km for cases A1, A2, and A3. It can be seen from the figure that the start-up transient waves propagate both upstream and downstream at faster speeds than the convective cells. In Fig. 4a (case A1, $U = 2.5$ m s^{-1}), several convective cells produced by the upstream and downstream propagating gust fronts form between these two gust fronts. Cold-air outflow accompanies the precipitation system, spreading outward from the initial forcing center near the surface. Convective cells produced by these two gust fronts are advected by

TABLE 1. Characteristics of flow over convective systems with no mountain: $N_w = 0.006\ s^{-1}$, CAPE = 2049 $m^2\ s^{-2}$. Case A11 is simulated with a finer resolution (i.e., $\Delta x = 1$ km).

Case	U	c_d	Upstream propagating density current
A1	2.5	8.06	Yes
A2	9	8.82	Yes
A3	12.5	9.77	No
A4	1	7.14	Yes
A5	2	5.124	Yes
A6	5	7.94	Yes
A7	8.5	8.95	No
A8	9.5	8.72	Yes
A9	10	9.01	No
A10	15	10.0	No
A11	2.5	10.128	Yes

the midlevel inflow. In Fig. 4b (case A2, $U = 9$ m s^{-1}), a quasi-stationary upstream gust front occurs near $x = 25$ km. A quasi-stationary convective system is advected downstream by the background wind. This convective system is formed by the convective cells generated at the gust fronts. In Fig. 4c (case A3, $U = 12.5$ m s^{-1}), both the upstream gust front and the convective cells propagate downstream by the strong basic wind.

The first convective system initiated by the buoyancy force associated with the warm bubble can generate outward-propagating gravity waves, and the gravity waves then, in turn, may trigger new convective cells under favorable conditions. Since the mechanisms are similar in all of the warm-bubble simulations, only case A1 will be discussed further. Figure 5 illustrates the potential temperature, vertical velocity, rainwater content, and cold-air outflow boundary at 3-min intervals for case A1. At earlier times, such as from 99 to 108 min, the cold-air outflow forms and spreads outward (leftward and rightward) from the warm bubble center near the surface. The updrafts generated by gust fronts and triggered by gravity waves associated with the convection merge together before $t = 99$ min and then separate into two parts. The updrafts generated by gravity waves propagate with a faster speed than those of the gust fronts and disperse or dissipate at a later time. This phenomenon can be explained by the description of the propagating mode associated with gravity waves proposed by Lin et al. (1998) and sketched in Fig. 2. The lack of growth for the propagating mode is due to the more stable environment, which instead leads to propagation relative to the flow (i.e., no critical levels present).

When the forcing due to the density current becomes dominant at later times (Figs. 5e–h), the updrafts produced by the gust fronts grow, while they are advected by the midlevel inflow and cut off by their compensating downdraft. The updrafts show different development and propagation modes from those of Figs. 5a–d. This evolution corresponds to the growing mode within a multicell storm (Lin et al. 1998; Fig. 2), which is caused

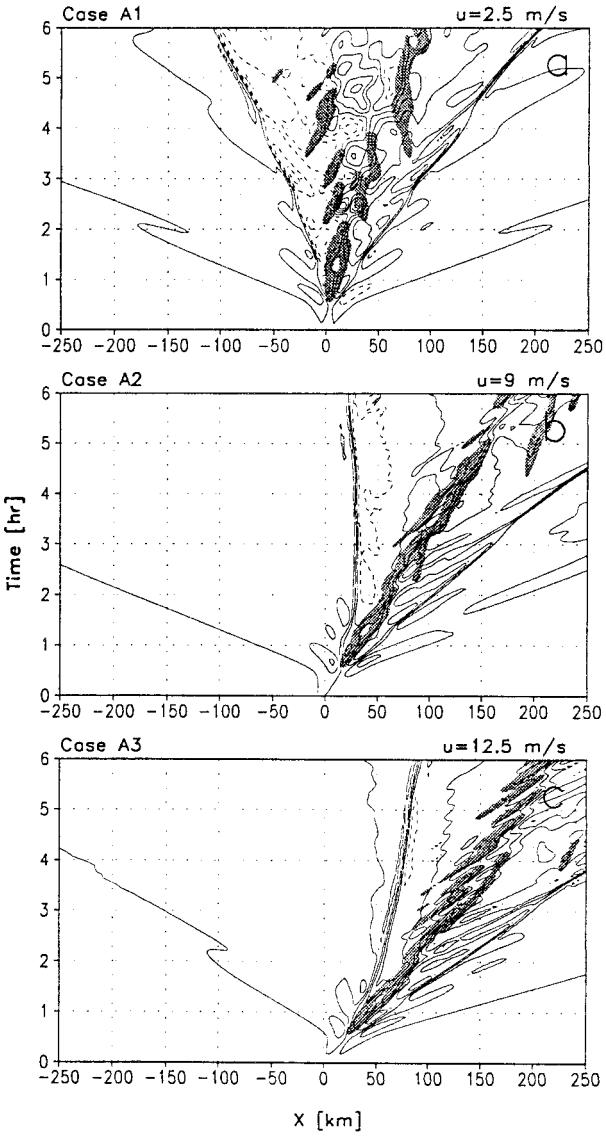

FIG. 4. Time evolution of surface wind and the rainwater at $z = 1$ km. The contour interval for surface wind is 5 m s^{-1}. Rainwater greater than 0.5 g kg^{-1} is shaded. Positive (negative) values are in solid (dashed) lines. Three cases are shown: (a) A1 ($U = 2.5$ m s^{-1}), (b) A2 ($U = 9.0$ m s^{-1}), and (c) A3 ($U = 12.5$ m s^{-1}).

by the steering level propagation in a conditionally unstable environment. Precipitation accompanying the cells can also be found behind the gust fronts. In case A1, all of the convection exhibits a symmetric pattern due to the weak flow and lack of vertical shear. Case A11 (see Table 1) is a sensitivity experiment with a finer resolution, $\Delta x = 1$ km. With this resolution, stronger evaporative cooling associated with precipitation is generated. It is also found that several cells develop in this multicell storm. The mechanisms for the cell generation, development, and propagation are similar to those in case A1 except that the rainfall is stronger.

For a well-developed upstream propagating density

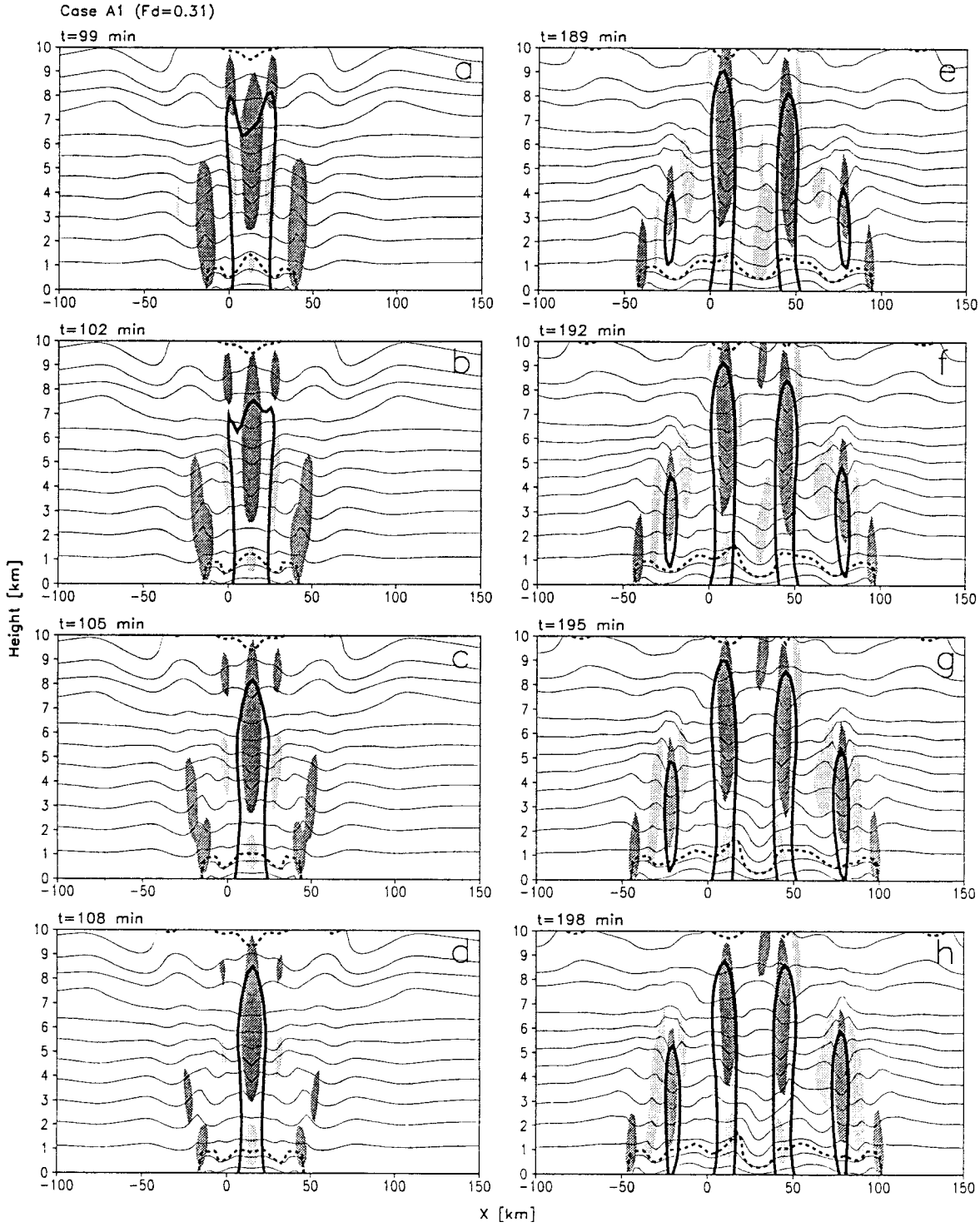

FIG. 5. (Case A1) Vertical cross section of the potential temperature (thin solid), vertical velocity (>0.5 m s^{-1}, dark shaded; <0.5 m s^{-1}, light shaded), rainwater (≥ 0.5 g kg^{-1}, thick solid), and the boundary of density current (-1 K, bold dashed) are present in every 3 min for case A1. Here (a)–(d) are for earlier stages and (e)–(h) are for later stages. The contour interval for potential temperature is 3 K.

current, the cell regeneration in our simulation is quite consistent with the advection mechanism proposed by Lin et al. (1998), even though uniform wind profiles are used. In order to establish the nature of the cell regeneration mechanism, they replaced the density current by a plateau and found that convective cells can still be generated. Our present simulation also demonstrates that the low-level shear is not essential in the generation of convective cells in this case. A thorough discussion of the multicell generation, development, and propagation mechanisms can be found in Lin et al. (1998) and have been briefly reviewed in section 1 of this paper.

4. Generation and propagation of convective systems over a mountain and moist flow regimes

For moist airflow over a mesoscale mountain, we need to determine when the airstream becomes blocked such that the ambient flow can be balanced by the reversed flow. Following procedures similar to those of Lin and Wang (1996), we find the critical Froude number (F_c) for upstream blocking is about 0.5 in dry simulations using the ARPS model. New convective cells can be triggered by the density current produced by the evaporative cooling associated with convective systems. Thus, an additional flow parameter, namely, the thermal Froude number, may come into play. However, due to the complicated evaporation process, it is not straightforward to estimate the cooling rate necessary to define this thermal Froude number. The thermal Froude number may be directly related to the CAPE, which can be estimated from the upstream sounding. However, in this study we will focus our discussions on the moist Froude number (F_w), which ranges from 0.208 to 2.083. Note that wave breaking aloft is also possible in this range of F_w. Flow parameters and characteristics of cases simulated for a moist airstream over a two-dimensional mountain are summarized in Table 2.

TABLE 2. Characteristics of a moist airflow over 1 two-dimensional mountain. $N_w = 0.006\ s^{-1}$, $h = 2$ km, CAPE $= 2049\ m^2\ s^{-2}$.

Case	U	F_w	Upstream propagating density current
B1	2.5	0.208	Yes
B2	4.25	0.354	No
B3	10	0.833	No
B4	20	1.667	No
B5	3	0.250	Yes
B6	3.5	0.292	Yes
B7	3.9	0.325	Yes
B8	4	0.333	Yes
B9	4.1	0.341	No
B10	4.2	0.350	No
B11	4.5	0.375	No
B12	5	0.417	No
B13	7	0.583	No
B14	7.2	0.600	No
B15	7.4	0.617	No
B16	7.5	0.625	No
B17	12.5	1.042	No
B18	15	1.250	No
B19	25	2.083	No

From these numerical experiments, three moist flow regimes may be identified: (I) upstream propagating convective system, (II) stationary convective system, and (III) both stationary and downstream propagating systems. The characteristics and dynamics of these moist flow regimes will be explained below.

Figure 6 illustrates the time evolution of rainwater content ($\geq 0.5\ g\ kg^{-1}$) at the height of $\sigma = 1$ km and the horizontal wind speed (contour lines of -5, 0, and $5\ m\ s^{-1}$) for all cases in experiment series B. The moist Froude numbers and basic flow speeds are 0.208 and $2.5\ m\ s^{-1}$ (case B1), 0.292 and $3.5\ m\ s^{-1}$ (case B6), and 0.333 and $4.0\ m\ s^{-1}$ (case B8), respectively. When F_w increases from 0.208 to 0.333 ($U = 2.5$ to $4.0\ m\ s^{-1}$), the overall convective system is able to propagate upstream of the mountain. The embedded, individual convective cells are generated over the upslope, which then propagate downstream once they form (Figs. 6a–c). These cases may be classified as the *upstream propagating flow regime* (regime I) since the new cells are still being generated by the gust front updraft that moves upstream. The individual convective cells more likely form and grow repeatedly on the upslope due to an upstream propagating density current and then dissipate while they propagate downstream. In order to understand the formation mechanisms of these convective cells, we plot the vertical cross section of potential temperature, vertical velocity, rainwater content, and density current at 6-min intervals for case B1 (Fig. 7). From Figs. 7a–d, we can see that a convective cell is triggered by the GFU produced by the mountain-induced convective system near the mountain peak, which is similar to that shown in Fig. 2. Once this new cell forms, it propagates slightly downstream, grows, and then merges with the mountain-induced convective system (Figs. 7e–h; also see Fig. 8c). After the merging, the density current propagates upstream against the basic flow and triggers another new cell at the gust front, which then starts to propagate downstream (rightward) along the windward slope (Figs. 7i–l). At $t = 498$ min, the gust front has already propagated to a distance of $x = -170$ km. The precipitation associated with this type of convective system may be responsible for some of the heavy rainfall or even flash flood events over the windward slope and plain area since the overall convective system may last for a long time. It appears that the formation of individual convective cells is dominated by the density current forcing at the later stage, when the density current is fully developed. This sequence of events is similar to that found in case A1 (Figs. 5e–h). No convective cells are able to form on the lee slope in this case (Figs. 6a and 7).

With a more careful inspection of the areas of heavy precipitation shown in Figs. 6a–c and 7, it becomes

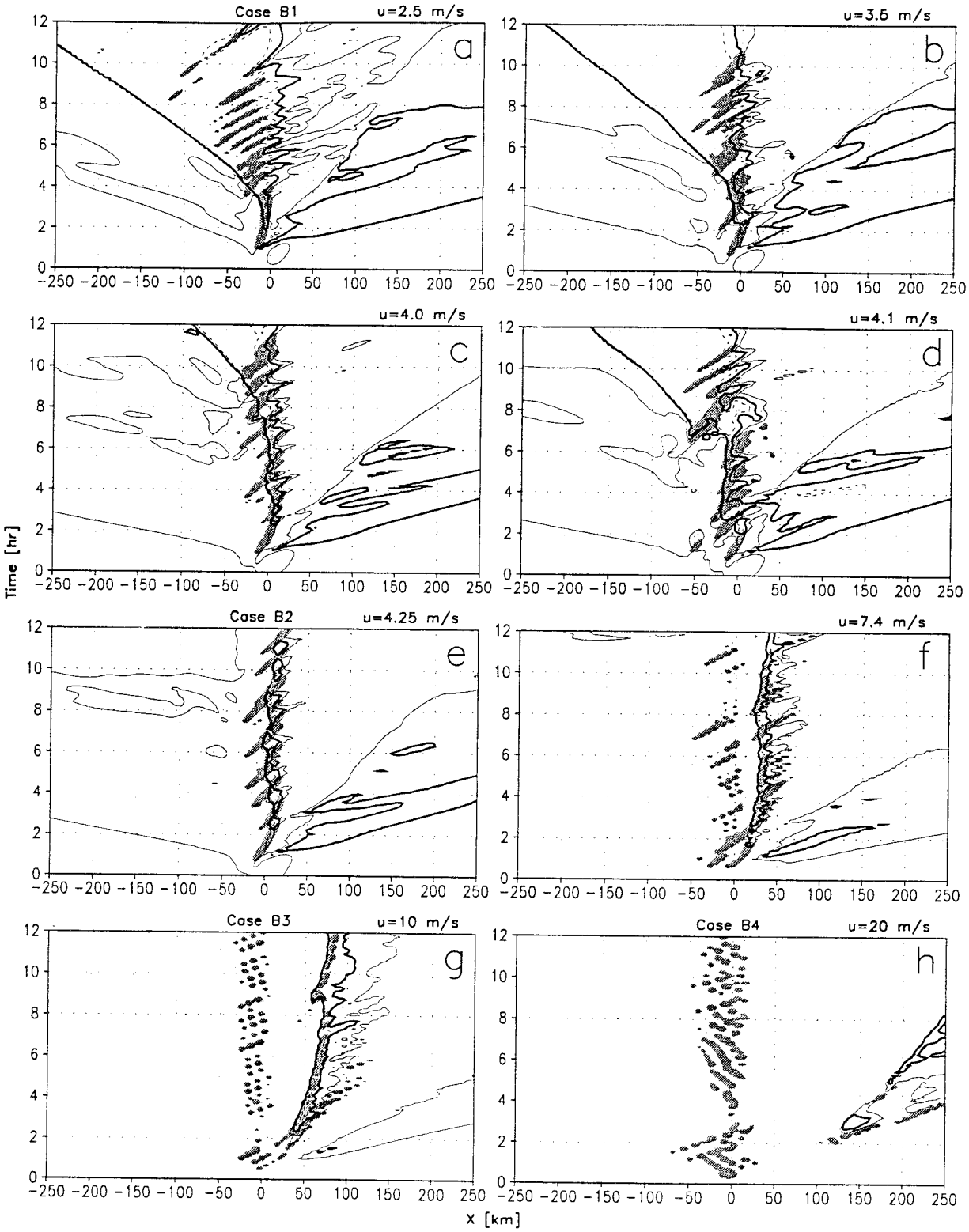

FIG. 6. Time evolution of surface wind (contour lines in −5, 0, and 5 m s^{-1}) and rainwater content (≥0.5 g kg^{-1}, shaded) at σ = 1 km for regime I (a)–(c), regime II (d)–(e), and regime III (f)–(h). Positive (negative) values are solid (dashed) for horizontal velocity. The corresponding values of U and F_w are (a) 2.5 m s^{-1} and 0.208, (b) 3.5 m s^{-1} and 0.292, (c) 4.0 m s^{-1} and 0.333, (d) 4.1 m s^{-1} and 0.341, (e) 4.25 m s^{-1} and 0.354, (f) 7.4 m s^{-1} and 0.617, (g) 10 m s^{-1} and 0.833, and (h) 20 m s^{-1} and 1.667.

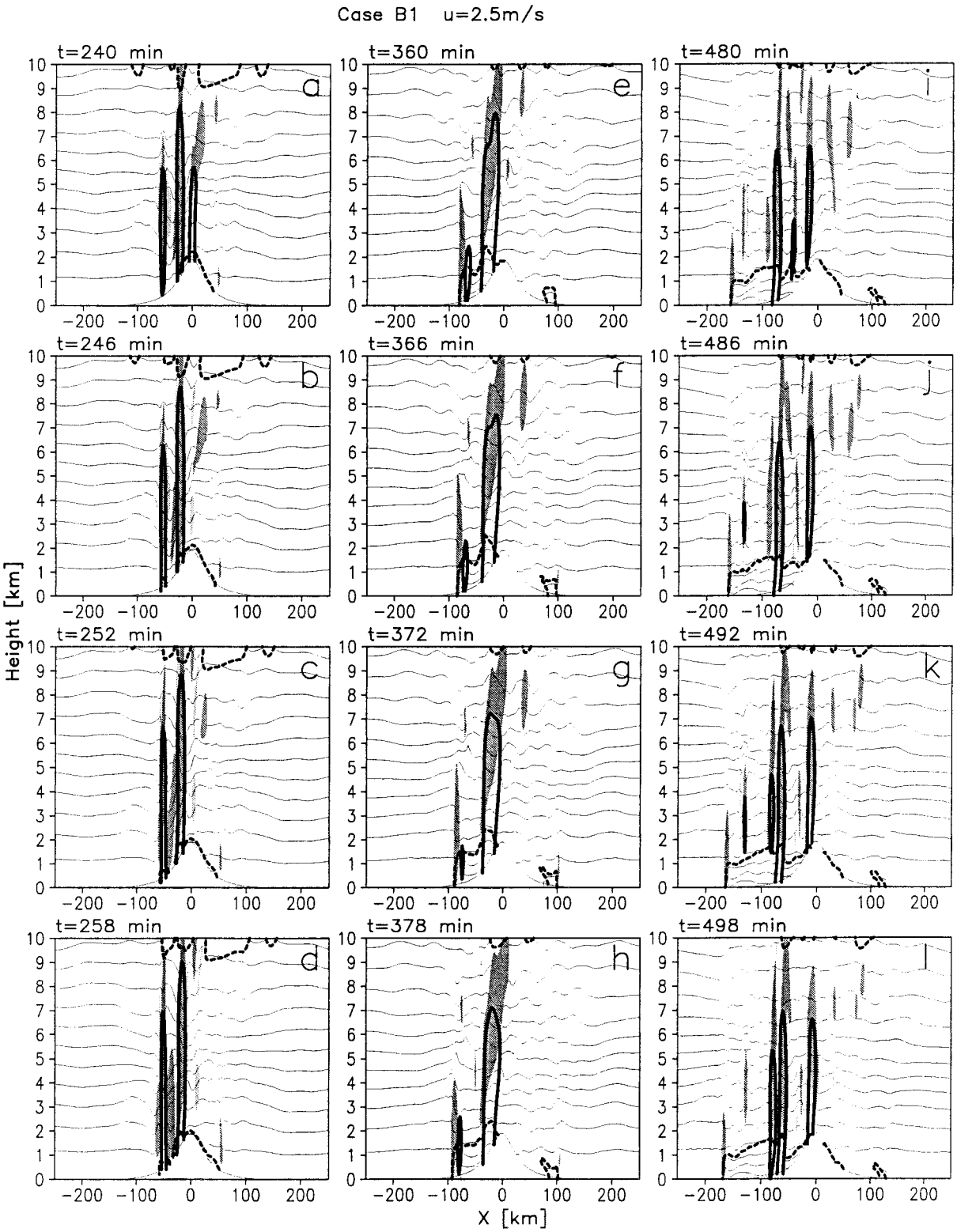

FIG. 7. (Case B1, regime I.) Vertical cross sections of the potential temperature (thin solid with a contour interval of 3 K), vertical velocity ($w > 0.5$ m s^{-1} heavy shaded; $0 < w < 0.5$ m s^{-1} light shaded), rainwater content ($\geq$0.5 g kg^{-1}, thick solid), and the boundary of density current (-1 K, bold dashed) are shown at 4-min intervals in each column for case B1 ($F_w = 0.208$). The basic flow speed (U) is 2.5 m s^{-1}.

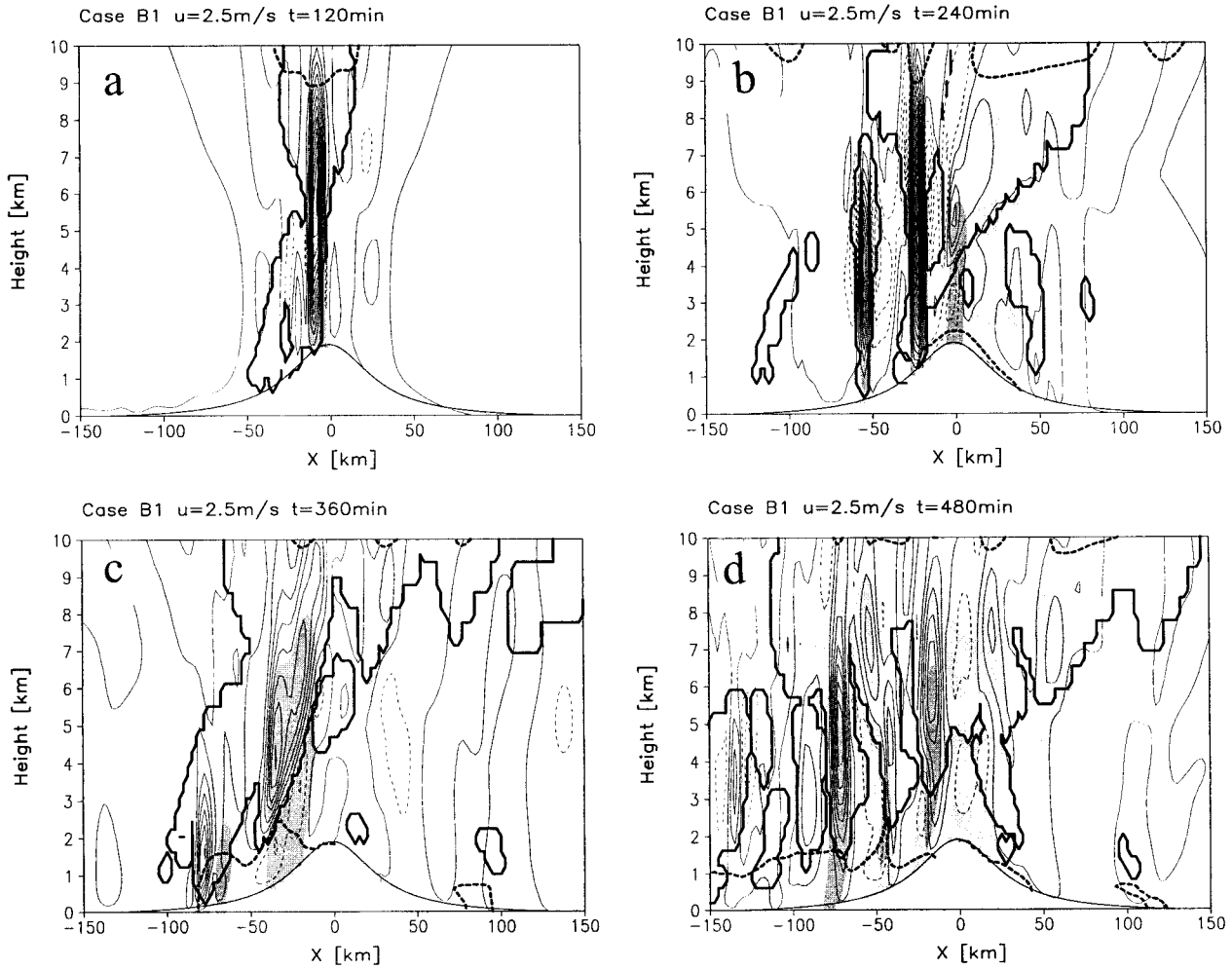

FIG. 8. Detailed plots of vertical cross sections of the cloud boundary (thick lines, $q_c > 0$), vertical velocity (positive, thin solid; negative, thin dashed; contour is 0.5 m s^{-1}), rainwater content ($0.05 < q_r < 0.5$ g kg^{-1}, light shaded; $q_r \geq 0.5$ g kg^{-1} heavy shaded), and the boundary of density current (-1 K, bold dashed) are shown for $t =$ (a) 2 h, (b) 4 h, (c) 6 h, and (d) 8 h. In order to show the details of flow circulations, only a portion of the domain (-150 km $< x <$ 150 km) is plotted.

evident that they always occur at the foothill and the upslope area of the mountain, even though the individual cells may be triggered farther upstream. This implies that the convergence associated with the orographic forcing plays an important role in enhancing first the convection and then the precipitation over the upslope area and in the vicinity of the foothill. This also indicates that a wave induced conditional instability of the second kind (wave-CISK; Hayashi 1970; Lindzen 1974) mechanism may operate in the combined orographic forcing and elevated thermal forcing. Using a coupled theoretical model with a CISK-like heating, Davies and Schar (1986) extended the studies of the combined effects of thermal forcing associated with orographic clouds and orographic forcing (e.g., Smith and Lin 1982; Raymond 1972). They found that the elevated thermal forcing and orographic forcing may interact with each other, enhance the response upstream, and produce strong lee slope winds. As pointed out by Davies and Schar (1986), the enhanced response is indeed a resonant wave-CISK mode. Although the wave-CISK mechanism may play an important role in the present case, the model of Davies and Schar cannot be applied directly due to the lack of precipitation and some other constraints in their model. In the present case, the precipitation appears to play an essential role by producing evaporative cooling which, in turn, produces the density current and gust front and then generates new convective cells.

Another interesting feature revealed by Figs. 6a–c is that rainfall occasionally occurs ahead of the density current. In order to study the mechanism for producing this and more detailed structures of the convective system, we show the vertical velocity, cloud boundary, rainwater content, and density current for $t = 2$, 4, 6, and 8 h (Fig. 8). In the early stages, such as $t = 2$ h, the convective system is mainly located on the upslope region near the mountain peak. One major convective cell is located near the mountain peak, while a much

weaker cell with minimal embedded rainwater can be identified on the upstream side of the major convective cell. The overall convective system (denoted by the cloud boundary in Fig. 8) extends upstream on the upslope side to $x = -50$ km. At $t = 4$ h (Fig. 8b), there exists roughly three major convective cells within the convective system, with the strongest convective cell located at $x = -20$ km, a weaker cell located at $x = -50$ km, and a very weak cell located over the lee slope at $x = 40$ km. A weaker convective cell is located at $x = -125$ km, which apparently is produced by the gravity waves generated by the elevated latent heating from the convective system over the upslope. By comparing Figs. 7 and 8, it becomes apparent that the convective cell over the lee slope is advected from the upslope, but is weakened by the downslope adiabatic warming. However, the overall convective system is broadened by a new cell generated at the hydraulic jump over the lee slope. Note that the convergence produced by the hydraulic jump over the lee slope is quite strong. The upstream cell appears to be enhanced by gravity waves or disturbances produced by the major convective cell (Fig. 7), as evidenced by the lack of a well-defined density current over the upslope, and then propagates down the windward slope. All of the convective cells mentioned above produced rainfall, and the major cells produced heavy rainfall.

At a later time, such as $t = 6$ h (Fig. 8c), the convective cells are weakened slightly, but broadened in horizontal area. It becomes very clear that new cells are being generated by the density current over the upslope. As mentioned above, this generation mechanism becomes dominant at later stages of the convective system development. Note that these new cells will propogate downstream and develop into stronger cells (Figs. 7a and 8). It is noteworthy that some narrow downdrafts exist between the strong updrafts within the multicell system, which is consistent with the conceptual model of orographic rain proposed by Smith (1979) and Lin (1993), which exhibits a closely packed convection. At $t = 8$ h (Fig. 8d), there are more convective cells embedded within the overall convective system. It can be readily identified that there are four cells located over the upslope and the plain area upstream, while there are three very weak cells located over the lee slope and the plain area downstream. The cells located near the mountain peak and at $x = -75$ km produce heavy rainfall. The density current has already propagated to $x = -160$ km at this time. As in Fig. 6a, there always exist several convective cells over the upslope and plain area that may be viewed as a single convective system, although these embedded cells are generated at the gust front and propagate up the windward slope (downstream with respect to the basic wind). As time progresses, this convective system with embedded convective cells may produce heavy accumulated rainfall from individual convective cells over the upslope and plain area upstream. The formation mechanism of the convective cells and the convective system is similar to that of case A1. The cell regeneration mechanism is the same as that proposed by Lin et al. (1998), although it is modified by the additional convergence induced by the orographic forcing.

When F_w increases to 0.341 and 0.354 (Figs. 6d,e), in which $U = 4.1$ and 4.25 m s^{-1}, respectively, the density current becomes stationary (at least before $t = 6$ h for the case with $U = 4.1$ m s^{-1}). Figure 9 illustrates the vertical cross sections of potential temperature, vertical velocity, rainwater content, and density current at 6-min intervals for earlier and later stages of case B2 ($U = 4.25$ m s^{-1}, $F_w = 0.146$). From $t = 75$–93 min, new cells are triggered by the gravity waves associated with the mountain-induced convective system on both sides of the old cells (Figs. 9a–d). However, these new cells do not grow further and may be classified as the propagating mode proposed by Lin et al. (1998, Fig. 2). When the convective system moves to the downslope side, a new cell with rainwater content greater than 0.5 g kg^{-1} is strengthened at midlevels over the upslope of the mountain by the gravity waves associated with the convective system (Figs. 9e–h and 10a). It may be classified as the growing mode of a convective cell proposed by Lin et al. (1998, Fig. 2). Meanwhile, the old cell is weakened when it moves downstream over the lee slope due to adiabatic warming (Figs. 9i–l). At $t = 162$ min, the new cell takes its place and becomes a dominant convective cell. These processes are repeated over the mountain peak for several hours. Due to this cell regeneration process, the overall convective system remains stationary over the mountain, which is also evident from Fig. 10.

It appears that the overall convective system is maintained by a balance between the orographic forcing and the cold-air outflow forcing, since the density current becomes stationary with respect to the mountain (Figs. 6d,e and 10). Thus, this flow regime may be classified as the *quasi-stationary convective system regime* (regime II). In this flow regime, the stationary convective system may be able to produce heavy accumulated rainfall from individual convective cells propagating in the vicinity of the mountain peak. Note that the strongest convective cells are located near the mountain peak, while those produced by the density current upstream are very weak at their earlier stage. Comparing all cases of regimes I and II (Figs. 6a–e) reveals that strong convective cells (e.g., $q_r > 0.5$ g kg^{-1}) are always present over the upslope or near the mountain peak instead of farther upstream on the plain area, which indicates the importance of the phasing of orographic forcing and gravity wave forcing, which are essential for the the new cell to develop into a strong cell.

When F_w increases to values larger than 0.354 ($U = 4.25$ m s^{-1}), the generation and propagation of the convective system (Figs. 6f–h) are significantly different from the first two flow regimes (Figs. 6a–e). This flow regime may be classified as regime III, which possesses

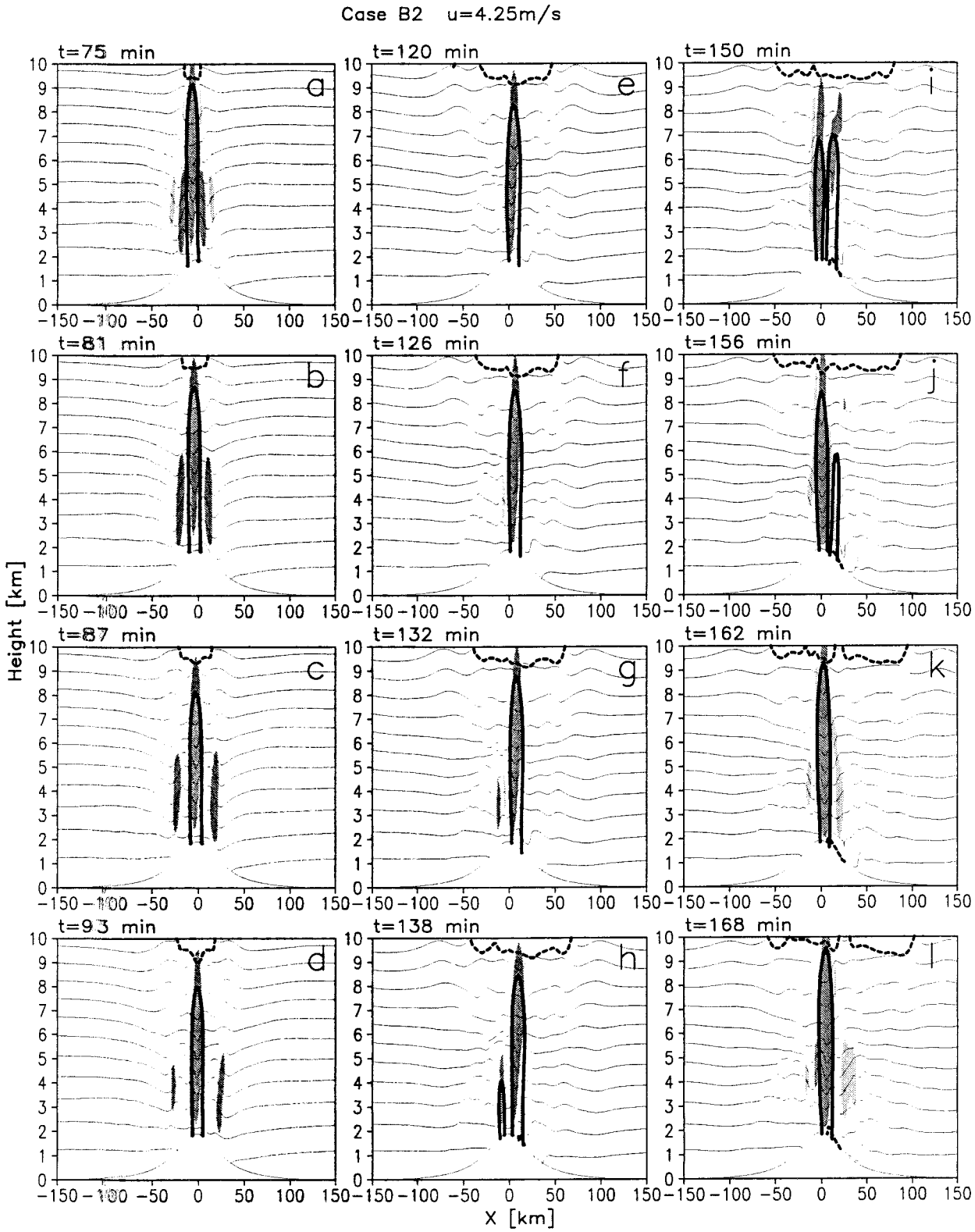

FIG. 9. (Case B2, regime II.) Same as Fig. 7 except for with $U = 4.25$ m s^{-1}.

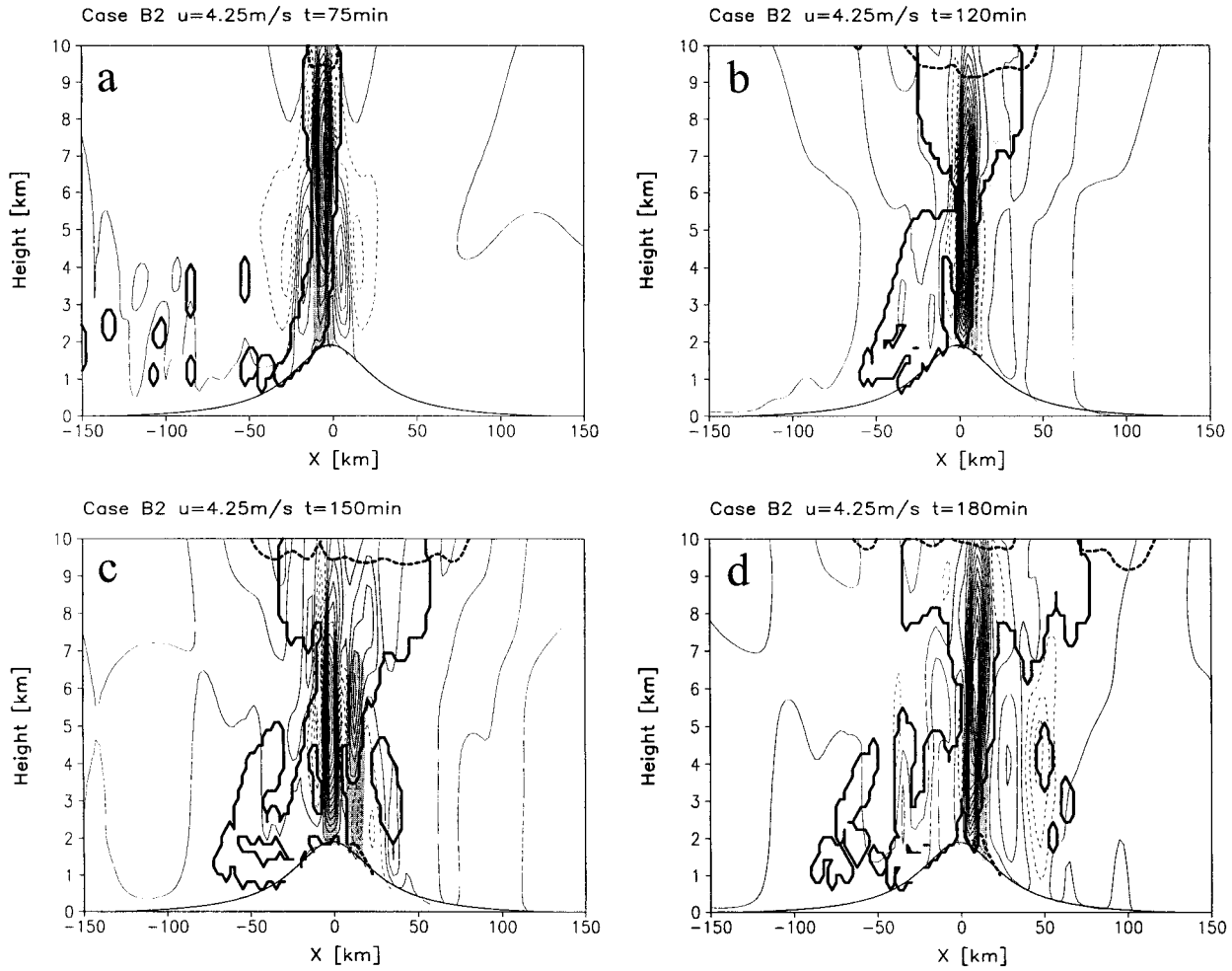

FIG. 10. Same as Fig. 8 except for case B2.

two quite distinct modes based on the generation and propagation of the convective systems: *the quasi-stationary system* and the *downstream propagating system* (Figs. 6f–h). For the stationary convective system, the cell generation is similar to that of regime II. Figures 11a–d show the vertical cross sections of potential temperature, vertical velocity, rainwater content, and cold-air region at 6-min intervals for case B3 ($F_w = 0.833$, $U = 10$ m s^{-1}). At $t = 30$ min (Fig. 11a), a convective cell is triggered by the convergence associated with orographic forcing and then develops over the windward slope at $x = -40$ km. From $t = 36$–48 min (Figs. 11b–d, two new cells are apparently enhanced by gravity waves associated with the older convective cells. The development of these two convective cells can be explained by the growing mode of convective cells (Lin et al. 1998, Fig. 2). This mechanism continuously promotes the development of convective systems over the windward slope, where cold-air regions above the convective cells are produced by the detrainment associated with air parcels overshooting their level of neutral buoyancy near the tops of convective cells.

Analysis of the water vapor field (not shown) shows water vapor in cold-air regions is less than 4 g kg^{-1}, which is close to a dry environment. In a case study in TAMEX, Chen et al. (1991) suggested that new convective cells can be formed continuously along the western slope of a mountain in northern Taiwan and move eastward to merge into the western flank of the quasi-stationary precipitation system over the lee slope. Their case may fall into our regime III, and the formation and propagation mechanisms for convective cells discussed in their case may also be explained by Lin et al. (1998, Fig. 2).

For the downstream propagating system of regime III, the evaporative cooling associated with falling precipitation appears to play an important role in new cell generation over the lee slope. This is clearly shown in Figs. 11e–h and Fig. 12a, when the main convective system is propagating downstream. A new cell generated upstream crosses over the mountain peak and merges with the main convective system over the lee slope. The updraft produced by the western flank of the gust front on the lee slope triggers a new convective cell.

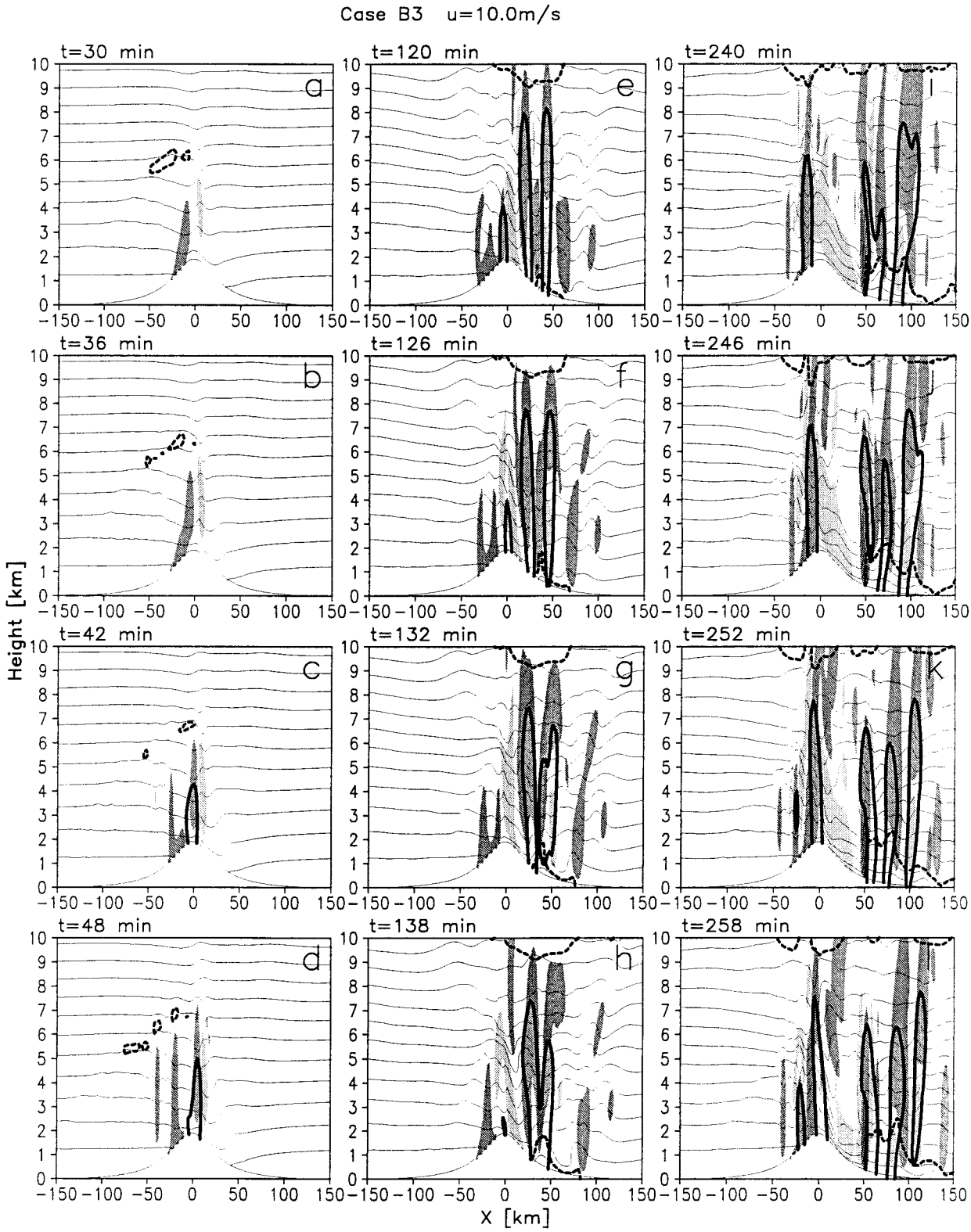

FIG. 11. (Case B3, regime III.) Same as Fig. 7 except for with $U = 10.0$ m s^{-1}.

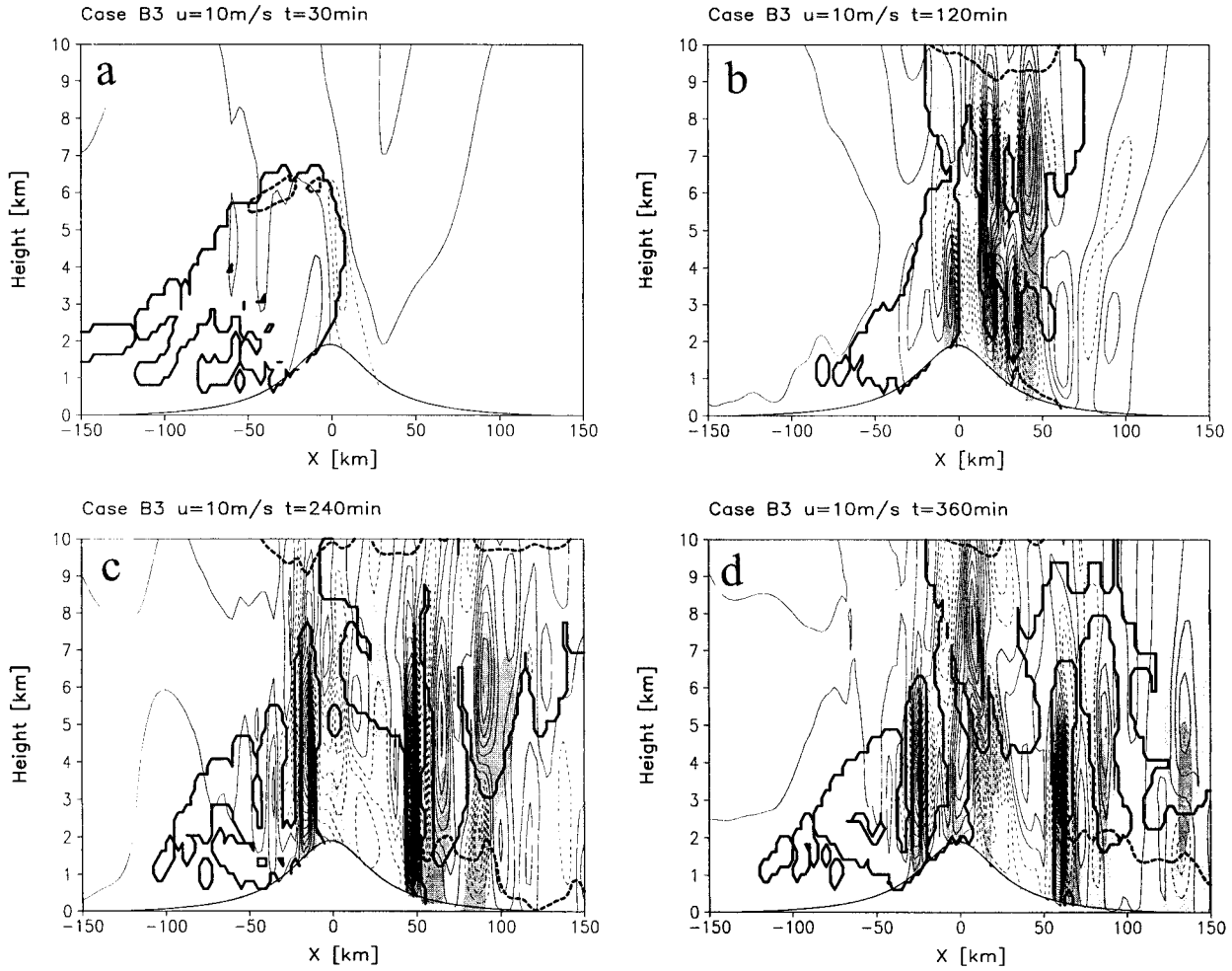

FIG. 12. Same as Fig. 8 except for case B3.

For t = 240–258 min (Figs. 11i–l and 12c,d), a rain-shadow region forms in between the stationary convective system and the downstream propagating convective system over the lee slope. Near the foothill on the lee side, the updraft produced by convergence associated with the downslope wind and gust front is strengthened by wave breaking aloft, which is located at about $0.85\lambda_z$, that is, 3.7 km (e.g., Lin and Wang 1996). During this period, the internal hydraulic jump and the gust front play important roles for the development of the downstream propagating convective system.

In regime I, the mountain and gravity waves are the main forcing mechanisms for new cell formation at earlier stages. At later stages, the density current develops and becomes the dominant forcing. The cell regeneration mechanism can be explained by Lin et al. (1998). As F_w increases, the convective system becomes quasi-stationary with both embedded convective cells and the gust front located over the mountain peak and windward slope of the mountain (regime II). In this flow regime, a balance between the orographic forcing, gravity waves generated by elevated latent heating, and the cold-air outflow has been reached. When F_w increases further (to regime III), two modes of convective systems were found: a quasi-stationary system and a downstream propagating system. For the quasi-stationary system, the cell regeneration is similar to that of regime II. For the downstream propagating system, the convergences generated by both the internal jump and the gust front play important roles for the cell generation.

Figure 12 shows the vertical velocity, cloud boundary, rainwater content, and density current for t = 0.5, 2, 4, and 6 h, providing more detailed structures of the convective system for case B3, compared with Fig. 11. At an early stage, such as t = 2 h (Fig. 12b), the major convective system is located in the vicinity of the mountain peak. However, the large convective cells have already climbed over the mountain peak and propagated to the lee slope at about x = 25 km. Two convective cells may be identified, with the downstream cell located near the western end of the lee side density current. At t = 4 h (Fig. 12c), there exist two distinct convective

TABLE 3. Summary of sensitivity tests of evaporative cooling processes. These cases may be compared with the control case B1.

Case	Characteristics	With evaporation
D1	Moist	No
D2	Moist after 3-h dry simulation	Yes
D3	Moist after 3-h dry simulation	No

systems, with one located over the upslope and the other located over the lee slope. The upslope convective system is weaker at this time, while the downslope one is much stronger. The strongest convective cell associated with the downslope convective system is located at the western edge of the downslope density current. At $t =$ 6 h (Fig. 12d), the upslope convective system redevelops to be as strong as the downslope system. At this stage, two distinct systems, that is, stationary and downstream propagating modes, can be seen clearly with about equal strength.

5. Sensitivity to evaporative cooling and upstream blocking

In section 4, we found that in regime I, the orographic forcing dominates at earlier stages, while the cold-air outflow or density current forcing dominates at later stages. In regime II, the orographic forcing is in balance with the gravity waves generated by elevated heating and the cold-air outflow forcing. Therefore, the convective system becomes quasi-stationary in the vicinity of the mountain peak. In regime III, in addition to the quasi-stationary convective system near the mountain peak, there exists a downstream propagating convective system that is generated by convergence formed by the downslope wind and the upstream gust front on the leeward side. It appears that the evaporative cooling and orographic forcing are both important in all of these regimes.

In order to isolate the effect of orographic forcing, we deactivate the evaporative cooling associated with the falling precipitation (case D1). Note that precipitation is still allowed in these experiments to prevent the thermal energy associated with the condensates from remaining in the cloud formation and then forming an unreasonably large orographic cloud. This differs from the study of Smith and Lin (1982), since they did not consider the evaporative cooling effects. Case D1 is identical to case B1 except with the evaporative cooling associated with the falling precipitation deactivated. In order to investigate the sensitivity of orographic convective system, we perform cases D2 and D3, which are equivalent to cases B1 and D1 except with the preexistence of upstream blocking. The upstream blocking in D2 and D3 is achieved by performing the corresponding dry simulations for 3 h before the moist processes are activated. Table 3 summarizes these sensitivity tests.

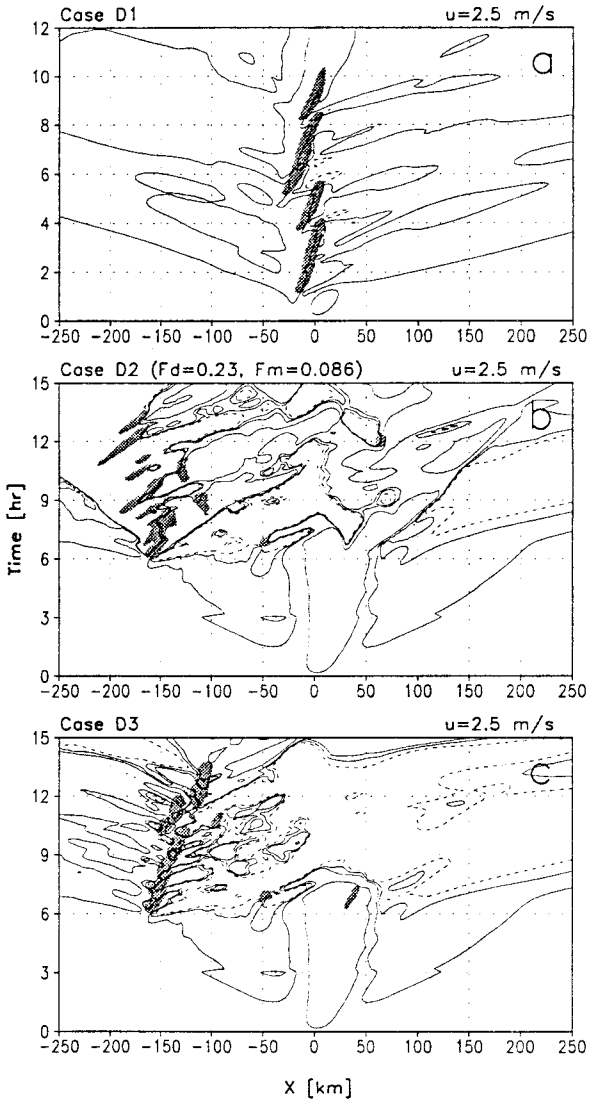

FIG. 13. As in Fig. 6 except for cases D1–D3 (see Table 3 for flow characteristics). The contour lines for case D1 are −5, 0, and 5 m s^{-1}, while they are −1.0, 1, and 5 m s^{-1} for cases D2 and D3.

In both cases D1 and D3, since the evaporative cooling is deactivated, no upstream propagating density current can form. However, case D2 does produce an upstream propagating density current, although the upstream blocking is weak. The phase speed of the gust front is 11.07 m s^{-1}, which is close to that of case B1 (10.42 m s^{-1}). Figure 13 illustrates the surface wind speed and the rainwater (>0.5 g kg^{-1}) fields for cases D1–D3. The contour lines in case D1 are −5, 0, and 5 m s^{-1}, while they are −1, 0, 1, and 5 m s^{-1} in cases D2 and D3. For case D1, since there is no significant pressure gradient associated with the evaporative cooling across the gust front, the convective cells generated upwind of the mountain are advected downstream slowly by the ambient flow (Fig. 13a). Unlike case B1, in which convective cells are triggered by the upstream

propagating density current (Fig. 6a), the convective cells in case D1 are triggered by the convergence associated with orographic forcing alone. The overall convective system is stationary and located over the upslope region near the mountain peak. Note that case D1 does not belong to regime I anymore. Based on the analysis of the vertical cross sections of potential temperature, vertical velocity, rainwater content, and the cold-air region at 6-min intervals (not shown), the mountain-induced convective cells still play a dominant role, although several cells are triggered by gravity waves associated with it.

For cases D2 and D3, the moist processes are introduced impulsively after $t = 3$ h in the dry simulation. The leading edge of the upstream convegence is located at $x = -52$ km at this time. As can be seen from Fig. 13, even though the upstream convergence is weak, it is able to trigger convection once the moist processes are activated. An upstream propagating deceleration line of $U = 1$ m s^{-1} is clearly shown in the figures (Figs. 13b,c). It initiates the convective cell located at $x = -160$ km at $t = 6$ h. In Figs. 13b,c, a negative horizontal wind speed area, which appears at $t \approx 5$ h and is located at $x = -52$ km, is associated with the upstream deceleration in the lower levels. Since the precipitation occurs upstream ($\sim$160 km) of the mountain, we hypothesize that the midlevel disturbance is initiated by upstream deceleration when the moist processes are activated at $t = 3$ h. When the density current is well developed and propagates upstream, it becomes the main generation mechanism for the convective cells. Figure 14 shows the vertical cross sections of potential temperature, vertical velocity, rainwater content, and the cold-air region at 6-min intervals for case D2. Since the interval of vertical velocity is 1 m s^{-1}, it is very difficult to see the disturbance initiated by the upstream deceleration.

From Fig. 13b and Figs. 14a–d, there exist two dominant disturbances both upstream ($x = -160$ km) and downstream ($x = 25$ km) of the mountain. The upstream part is initiated by the upstream convergence associated with flow deceleration, while the downstream part is generated by the midlevel wave breaking that occurs earlier. However, the disturbance upstream develops faster than that downstream, and no cell is formed between those two disturbances. From Figs. 14e–h, the cell located at $x = -160$ km is well developed and generates several gravity waves downstream. It is clear that the mountain-induced convective system does not form on the upslope of the mountain because the upstream deceleration zone has propagated farther upstream. This is different from case B1, in which the convergence associated by the orographic forcing is over the upslope and is dominant in the earlier time. A cold-air region produced by the evaporative cooling is formed at this time and spreads out both upstream and downstream (Figs. 14e–h). The upstream propagating density current will play a dominant role at later times, similar to case B1. At $t = 360$ min (Fig. 14e), a new cell is triggered by the gravity wave at $x = -100$ km. From $t = 402$ to 420 min (Figs. 14i–l), as the downstream cell is gradually dissipating, so is the cell over the upslope region of the mountain. The main convective cell associated with the cold-air outflow still grows continuously at $x = -160$ km. For case D3, the formation of the convective cell upstream is similar to that of case D2 during the first 3 h (Fig. 13c). After 3 h, this convective system propagates downstream slowly and has the same behavior as that of case D1.

From case D1, that is, without evaporative cooling, the mountain-induced convective system cannot trigger new cells far upstream because the main convective cell is advected downstream by the ambient flow. From cases D2 and D3, it is found that the convective system can be formed in the plain area far upstream of the mountain, instead of over the upslope of the mountain when the upstream deceleration occurs. This result agrees with the study by Grossman and Durran (1984) and Hong and Huang (1996). However, the Froude number in our study is much smaller than that of Grossman and Durran in which the Froude number is 1.25. Nonlinearity definitely plays an important role in our case. For the first convective system, it is generated by the effect of upstream deceleration. Unlike case B1, the cell is induced by the orographic deceleration associated with orographic forcing in cases D2 and D3. Again, once the density current is fully developed (Fig. 13b), it then becomes the dominant formation mechanism of the convective cells. Note that multicells are generated, which propagate downstream once formed. Without the evaporative cooling (Fig. 13c), the convective system tends to propagate downstream instead of upstream.

6. Concluding remarks

Effects of orography, cold-air outflow, and gravity waves on the generation and propagation of convective systems in a conditionally unstable airstream over a mesoscale mountain are studied using a two-dimensional, nonhydrostatic, nonlinear cloud model. Based on the propagation of convective systems induced by orographic and thermal forcing, three regimes are identified: (I) an upstream propagating convective system, (II) a quasi-stationary convective system, and (III) quasi-stationary and downstream propagating systems.

In regime I (low F_w, moist Froude number), convective cells are generated by upstream deceleration associated with orographic forcing and by gravity waves associated with convective cells over the upslope area and on the plain area upstream of the mountain at earlier stages. They are generated by the upstream propagating density current at later stages when the density current is fully developed. This is similar to results in cases with no mountain. In this flow regime, quasi-continuous and heavy rainfall is produced over the upslope and plain areas as individual convective cells are generated

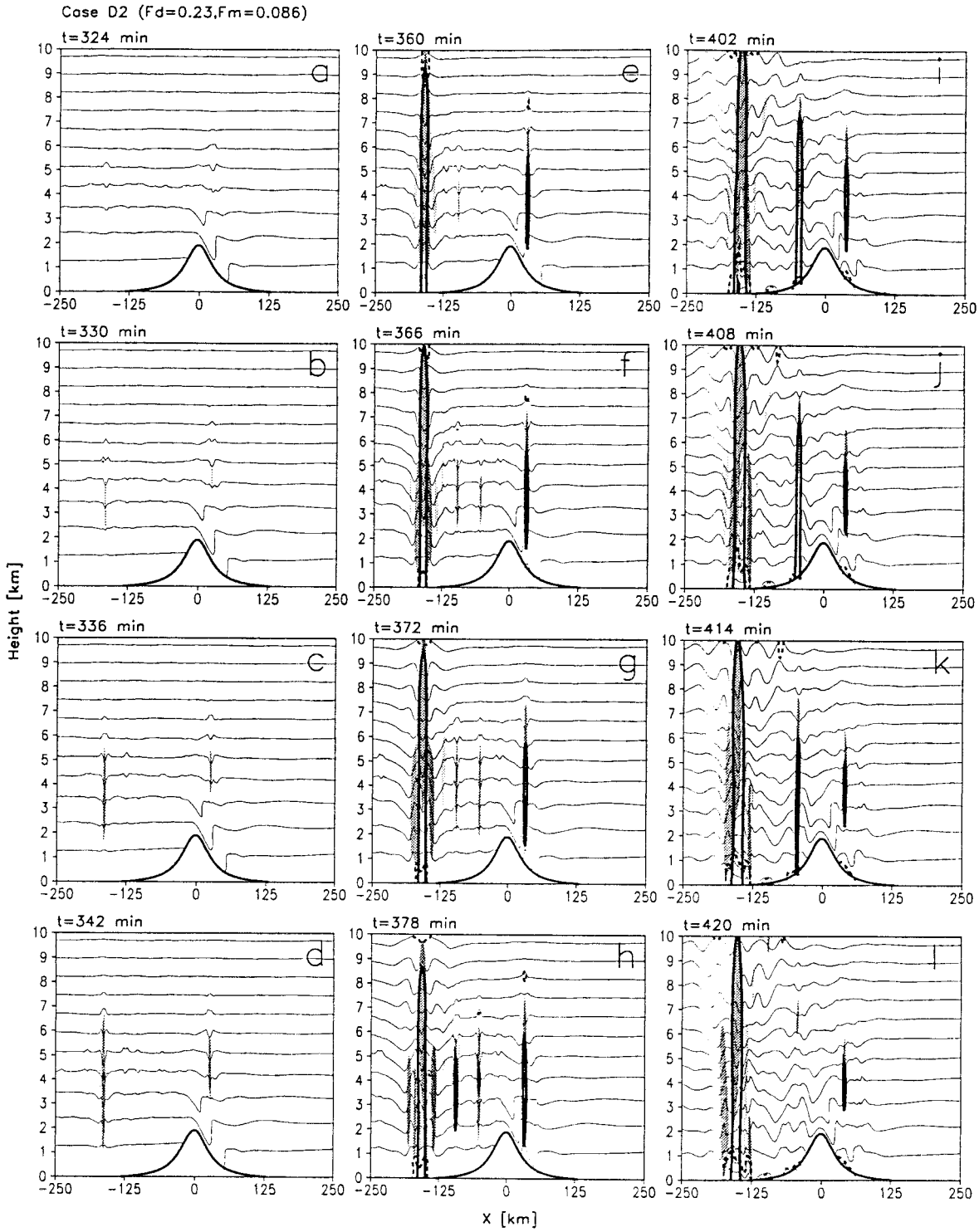

FIG. 14. As in Fig. 7 except for case D2.

farther upstream at the head of the density current and then propagate downstream once they form. No convective cells are able to form on the lee slope in this regime. This type of convective system may produce heavy rainfall over the windward slope and plain area. The individual cell regeneration, development, and propagation are explained by Lin et al. (1998). In the present cases, the precipitation plays an essential role

in producing evaporative cooling which, in turn, produces density current and gust front that generate new convective cells.

In regime II (moderate F_w), the convective system becomes quasi-stationary over the upslope and in the vicinity of the mountain peak. The individual convective cells are mainly generated by gravity waves associated with the mountain-induced convective system, orographic forcing and density current. A balance between the orographic forcing and the cold-air outflow forcing has been reached in this flow regime. In addition, the convective cells are able to merge into a large single cell due to the phasing of orographic forcing and gravity wave forcing.

In regime III (large F_w), two modes of convective systems can be identified: the quasi-stationary and downstream propagating modes. For the quasi-stationary convective system, its formation mechanisms are the same as those in regime II. For the downstream propagating convective system, the convective cells are mainly generated by the convergence associated with an internal hydraullic jump that propagates over the downslope of the mountain and produces heavy precipitation on the lee side. Under favorable conditions in a three-dimensional flow, this downstream propagating convective system may develop into a mesoscale convective complex.

In order to address the importance of evaporative cooling, we performed some sensitivity tests and found that without evaporative cooling, the mountain-induced convective system cannot trigger new cells far upstream of the mountain. The dominant convective system is advected downstream slowly by the basic flow. With the upstream deceleration, the convective system tends to occur far upstream on the plain rather than over the upslope area of the mountain. When the cold-air outflow is well developed, the upstream propagating density current becomes the dominant mechanism in triggering new cells upstream.

As mentioned in the text, new convective cells may be triggered by the density current produced by the evaporative cooling associated with convective systems. Thus, an additional flow parameter, namely, the thermal Froude number, may come into play. However, due to the complicated evaporation process, it is not straightforward to estimate the cooling rate in order to define this thermal Froude number. This thermal Froude number may be directly related to the CAPE, which can be estimated from the upstream sounding. Effects of CAPE on the generation and propagation of mesoscale convective systems over a mountain will be addressed in a separate study. It has been documented that diurnal forcing may enhance the convection during its development and produce heavy rainfall locally (e.g., Chen et al. 1991; Johnson and Bresch 1991; Akaeda et al. 1995). Johnson and Bresch (1991) found a pronounced diurnal variability in the rainfall during TAMEX. Therefore, studies with diurnal forcing are necessary to understand the dynamics of orographic rain in the real atmosphere. In addition, effects of bulk Richardson number, microphysical processes, and effects of vertical shear may also affect the formation and development of mesoscale convective systems, which also deserves a further study.

Acknowledgments. Discussions with Drs. Gerald Janowitz, Sethu Raman, and Vin Saxena at North Carolina State University and Dr. C.-S. Chen at National Central University in Taiwan are appreciated. The authors would like to thank Dr. Joseph Charney at NCSU for proofreading the manuscript and Yuqiu Zhu for help plotting figures. The help from Dr. M. Xue at University of Oklahoma on ARPS is highly appreciated. This work is partially supported by NSF Grant ATM-9224595. Some of the computations were performed on the workstations at the North Carolina Supercomputing Center.

APPENDIX

Estimate of the Moist Brunt–Väisälä Frequency

The moist Brunt–Väisälä frequency may be derived by (e.g., see Hess 1979; Iribarne and Godson 1981)

$$N_w^2 = \frac{g}{\overline{T}}(\Gamma_s - \Gamma), \tag{A1}$$

where Γ_s and Γ are the moist and actual lapse rates, respectively, and $\overline{T}$ the mean layer temperature. The moist lapse rate can also be derived by (see above references)

$$\Gamma_s = \frac{\Gamma_d\left(1 + \dfrac{Lw_s}{R_d T}\right)}{1 + \dfrac{L^2 w_s}{c_p R_v \overline{T}^2}}, \tag{A2}$$

where Γ_d is the dry lapse rate, w_s is the saturation mixing ratio of water vapor, L the latent heating, R_d the gas constant for dry air, c_p the heat capacity of constant pressure, and R_v the gas constant for water vapor. To estimate the Γ_s for Weisman and Klemp's sounding (Fig. 2), we focus on the lower layer from the surface to 850 mb, which gives the following values: $\overline{T} = 295$ K and $w_s = 10$ g kg^{-1}. With $L = 2.5 \times 10^6$ J kg^{-1}, $\Gamma_d = 10^{-2}$ K m^{-1}, $R_d = 287$ J kg^{-1} K^{-1}, $R_v = 61$ J kg^{-1} K^{-1}, and $c_p = 1004$ J kg^{-1} K^{-1}, the Γ_s can be roughly estimated from Eq. (A2) to be 5.1×10^{-3} K m^{-1}. With a rough estimate of $\Gamma = 4 \times 10^{-3}$ K m^{-1} from the sounding in the lower layer and Γ_s, $\overline{T} = 295$ K, Eq. (A1) gives the moist Brunt–Väisälä frequency (N_w) of 6×10^{-3} s^{-1}.

REFERENCES

Akaeda, K., J. Reisner, and D. Parsons, 1995: The role of mesoscale and topographically induced circulations in initiating a flash flood observed during the TAMEX project. *Mon. Wea. Rev.,* **123,** 1720–1739.

Chen, C.-S., W.-S. Chen, and Z. Deng, 1991: A study of a mountain-generated precipitation system in northern Taiwan during TAMEX IOP 8. *Mon. Wea. Rev.,* **119,** 2574–2606.

Davies, H. C., and C. Schar, 1986: Diabatic modification of airflow over a mesoscale orographic ridge: A model study of the coupled response. *Quart. J. Roy. Meteor. Soc.,* **112,** 711–730.

Droegemeier, K. K., and R. B. Wilhelmson, 1987: Numerical simulation of thunderstorm outflow dynamics. Part I: Outflow sensitivity experiments and turbulence dynamics. *J. Atmos. Sci.,* **44,** 1180–1210.

Grossman, R. L., and D. R. Durran, 1984: Interaction of low-level flow with the Western Ghats Mountains and offshore convection in the summer monsoon. *Mon. Wea. Rev.,* **112,** 652–672.

Hayashi, Y., 1970: A theory of large-scale equatorial waves generated by condensation heat and accelerating the zonal wind. *J. Meteor. Soc. Japan,* **48,** 140–160.

Hess, S. L., 1979: *Introduction to Theoretical Meteorology.* R. E. Krieger, 362 pp.

Hong, S.-S., and I.-C. Huang, 1996: Effects of topography and atmospheric stability on upstream heavy rainfall during Mei-Yu season. *Proc. Fifth National Conf. on Atmospheric Science,* Taipei, Taiwan, National Science Council, 580–585.

Houze, R. A., Jr., 1993: *Cloud Dynamics.* Academic Press, 573 pp.

Iribarne, J. V., and W. L. Godson, 1981: *Atmospheric Thermodynamics.* 2d ed. D. Reidel, 259 pp.

Johnson, R. H., and J. F. Bresch, 1991: Diagnosed characteristics of precipitation systems over Taiwan during the May–June 1987 TAMEX. *Mon. Wea. Rev.,* **119,** 2540–2557.

Jou, B. J.-D., 1994: Mountain-originated mesoscale precipitation system in northern Taiwan: A case study 21 June 1991. *Tao,* **5,** 169–197.

——, 1997: *Atlas of Radar Images of Mesoscale Convective Systems in the Taiwan Mei-Yu Season.* Department of Atmospheric Science, National Taiwan University, 144 pp.

Lin, Y.-L., 1993: Orographic effects on airflow and mesoscale weather systems over Taiwan. *TAO,* **4,** 381–420.

——, and H.-Y. Chun, 1991: Effects of diabatic cooling in a shear flow with a critical level. *J. Atmos. Sci.,* **48,** 2476–2491.

——, and T.-A. Wang, 1996: Flow regimes and transient dynamics of two-dimensional stratified flow over an isolated mountain ridge. *J. Atmos. Sci.,* **53,** 139–158.

——, R. L. Deal, and M. S. Kulie, 1998: Mechanisms of cell regeneration, development, and propagation within a two-dimensional multicell storm. *J. Atmos. Sci.,* **55,** 1867–1886.

Lindzen, R. S., 1974: Wave-CISK in the Tropics. *J. Atmos. Sci.,* **31,** 156–179.

Mueller, C. K., and R. E. Carbone, 1987: Dynamics of thunderstorm outflow. *J. Atmos. Sci.,* **44,** 1879–1898.

Raymond, D. J., 1972: Calculation of airflow over an arbitrary ridge, including diabatic heating and cooling. *J. Atmos. Sci.,* **29,** 837–843.

——, and R. Rotunno, 1989: Response of a stably stratified flow to cooling. *J. Atmos. Sci.,* **46,** 2830–2837.

Smith, R. B., 1979: The influence of mountains on the atmosphere. *Advances in Geophysics,* Vol. 21, Academic Press, 87–230.

——, and Y.-L. Lin, 1982: The addition of heat to a stratified airstream with application to the dynamics of orographic rain. *Quart. J. Roy. Meteor. Soc.,* **108,** 353–378

Smolarkiewicz, P. K., R. M. Rasmussen, and T. L. Clark, 1988: On the dynamics of Hawaiian cloud bands: Island forcing. *J. Atmos. Sci.,* **45,** 1872–1905.

Thorpe, A. J., M. J. Miller, and M. W. Moncrieff, 1982: Two-dimensional convection in nonconstant shear: A model of mid-latitude squall lines. *Quart. J. Roy. Meteor. Soc.,* **108,** 739–762.

Weisman, M. L., and J. B. Klemp, 1982: The dependence of numerically simulated convective storms on vertical wind shear and buoyancy. *Mon. Wea. Rev.,* **110,** 504–520.

Xue, M., K. K. Droegemeier, V. Wong, A. Shapiro, and K. Brewster, 1995: Advanced Regional Prediction System (ARPS) Version 4.0 user's guide. Center for Analysis and Prediction of Storms, University of Oklahoma, 320 pp. [Available online at http://www.caps.ou.edu/ARPS/ARPS4char.html.]

Yang, M.-J., and R. A. Houze, 1995: Multicell squall-line structure as a manifestation of vertically trapped gravity waves. *Mon. Wea. Rev.,* **123,** 641–661.